Engineering Fracture Mechanics 190 (2018) 134–145

Contents lists available at ScienceDirect

Engineering Fracture Mechanics

journal homepage: www.elsevier.com/locate/engfracmech

Effect of displacement rate and subcritical crack growth on *J*-R curves of API X65 steels in sour environment

C. Finamore [a,*], E.M. Castrodeza [a], J.E. Perez Ipiña [b], M.E. Cristea [c], M. Chekchaki [d]

[a] *Laboratory of Fracture Mechanics, COPPE Federal University of Rio de Janeiro, P.O. Box 68505, 21941-972 Rio de Janeiro, RJ, Brazil*
[b] *Fracture Mechanics Group, University of Comahue/CONICET, 8300 Neuquén, Argentina*
[c] *TenarisDalmine, Piazza Caduti 6 Luglio 1944, 1, 24004 Dalmine, BG, Italy*
[d] *Laboratory of H_2S, CO_2, and Corrosivity, National Institute of Technology INT, 20081-312 Rio de Janeiro, RJ, Brazil*

ARTICLE INFO

Article history:
Received 31 August 2017
Received in revised form 3 December 2017
Accepted 8 December 2017
Available online 9 December 2017

Keywords:
J-R curves
Sour environment
Displacement rate
Subcritical crack growth
API X65 pipeline steels

ABSTRACT

Fracture tests in sour solution of an API X65 steel for *J*-R curves determination were performed at different displacement rates. The results indicated a strong dependence of *J*-R curves on the displacement rate. At low displacement rates the *J*-R curves were affected by subcritical crack growth. Above a certain displacement rate, incubation time prior to subcritical crack growth was observed, being the experimental *J*-R curves not affected by this mechanism. A procedure to evaluate the contribution or not of subcritical crack growth to *J*-R curves of carbon steels in aggressive environments, verified for that specific steel-environment combination, is being proposed.

© 2017 Elsevier Ltd. All rights reserved.

1. Introduction

The growing demand of oil and gas industry, where exploration and production occur in deeper and more complex reservoirs, require a continue interest for developing materials with higher corrosion resistance and mechanical properties, especially for subsea equipment applications. The built wells in these reservoirs present a variety of technical challenges, and the most important one is related to sour environments, which may compromise the materials properties and consequently the equipment integrity [1,2].

Since pipeline steels are commonly employed in sour environments, their fracture characterization under aggressive conditions is very important for structural integrity control. The use of high strength low alloy steels with high fracture toughness, due to thermo-mechanical controlled manufacturing process [3], allows to manufacture thinner wall thickness pipes. However, these materials can suffer a severe degradation on fracture toughness when operating under aggressive environments.

Fracture behavior of carbon steels in sour environments has been studied by many authors [4–7]. Some researchers studied the effect of H_2S on the mechanical properties of a C-Mn pipeline steel. Some works [4] showed reductions of approximately 30% in the slope of *J*-R curves of a carbon steel immersed in sour environment compared to test results in air. Other researchers studied the hydrogen embrittlement effect on *J*-R curves of a high strength low alloy steel [5,6], tested in air with a load-line displacement rate of 30 mm/h, and at synthetic seawater with hydrogen charging, using a displacement rate of

* Corresponding author.
E-mail address: camila.finamore@metalmat.ufrj.br (C. Finamore).

https://doi.org/10.1016/j.engfracmech.2017.12.011
0013-7944/© 2017 Elsevier Ltd. All rights reserved.

Nomenclature

A_{pl}	plastic area under load versus load-line displacement curve
$a_{(i)}$	crack size at the *i* acquisition data calculated by DCPD
a_0	original crack size
a_p	physical crack size
a_{PD}	final crack size estimated by DCPD
B	specimen thickness
b_0	remaining ligament size prior to stable crack extension
C-L	specimen orientation in the pipe, where *C* (circumferential) is the direction perpendicular to the crack plane, and *L* (longitudinal) is the direction of crack front movement
E	modulus of elasticity in tension
EAC	environmentally assisted cracking
J	*J*-Integral
L-C	specimen orientation in the pipe, where *L* (longitudinal) is the direction perpendicular to the crack plane, and *C* (circumferential) is the direction of crack front movement
OD	outside diameter
P	load
P_i	initiation load
P_{th}	threshold load
SE(B)	single edge bend specimen
U_0	initial potential drop measurement
U	potential drop measurement
v	load-line displacement
v_f	final load-line displacement
W	specimen width
WT	wall thickness
y	half of potential gage span
Δa	crack extension
Δa_p	physical crack extension
Δa_{PD}	crack extension estimated by DCPD
η	plastic factor
σ_U	ultimate tensile strength
σ_{YS}	0.2% offset yield strength
BL	blunting line
DCPD	direct current potential drop
Q&T	quenched and tempered
SEM	scanning electron microscopy

0.1 μm/h. Results showed a considerable *J*-R curves drop when the steel was immersed in a corrosive environment. The authors associated this strength loss to the low displacement rate that led to longer period exposure and hence to higher hydrogen embrittlement effect [5–7].

This work focuses on the experimental *J*-R curves evaluation of an API X65 Q&T steel immersed in a sour environment. The crack growth was monitored by Direct Current Potential Drop (DCPD), which does not require a complex instrumentation, and has proven suitable for fracture testing in corrosive environments, with care to ensure that the applied current does not influence the electrochemistry and the crack growth rate [8,9].

Preliminary experimental tests on blunt notched SE(B) specimens in air and in the sour environment were carried out for adjusting DCPD parameters. No substantial differences between potential drop data obtained from both environments were found. This main result indicates the applicability of the DCPD technique in this specific aggressive environment without interference on the results. Those tests also showed an unexpected crack nucleation and propagation in blunt notch specimens (Fig. 1) when loaded at low load-line displacement rates (4.0×10^{-5} mm/s). This unexpected behavior indicated that the combination of material embrittlement and low displacement rates could lead to the possible coexistence of stable and subcritical crack growth mechanisms in monotonic fracture tests, where specimens with fatigue precracks are used.

To investigate this issue, fracture tests were carried out on precracked SE(B) specimens immersed in a sour environment at different load-line displacement rates. At this point, the main objective was to evaluate the existence of both stable and subcritical crack growth mechanism during monotonic fracture tests. A second objective was to study the possibility to separate the contribution of each crack growth mechanism. Finally, if these two mechanisms coexist and are separable, it will be

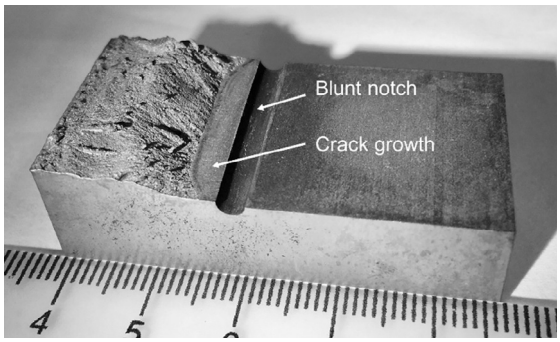

Fig. 1. Fracture surface of blunt notch specimen after testing. Nominal displacement rate of 4.0×10^{-5} mm/s.

possible to propose a methodology for fracture toughness characterization of this steel when immersed in such specific aggressive environment by *J*-R curves avoiding the subcritical crack growth contribution.

2. Experimental

2.1. Material

Fracture tests were performed on the base metal of a 508 mm (20 in.) nominal OD × 28.575 mm (1.125 in.) WT UOE API X65 Q&T steel pipe. Table 1 presents the chemical composition of the steel. The mechanical properties, obtained through round standard specimens according to ASTM E8 [10], in both longitudinal and transverse directions, are summarized in Table 2. The optical micrograph of the material, in the transverse orientation, is presented in Fig. 2, where can be observed a morphology featuring fine grains distribution of a microstructure consisting predominantly of ferrite.

2.2. Fracture tests

Monotonic fracture tests were carried out at different load-line displacement rates on single edge bend (SE(B)) $B \times 2B$ specimens (nominal $B = 24$ mm and $a/W \approx 0.5$) notched in L-C orientation [11,12]. The orientation of the specimens on the pipe can be seen in Fig. 3. Preliminary tests in air and in the specific environment indicated no significant differences in *J*-R curves between specimens removed from L-C and C-L orientations. As a result, the L-C orientation was chosen due to easier test specimen machining.

The specimens were fatigue precracked in air and then immersed in a sour environment that simulates seawater solution [13] saturated with a gas mixture of 25% concentrated H_2S balanced with CO_2, pH approximately 5, at room temperature and atmospheric pressure. Prior to loading, the specimens were soaked into the test solution for 48 h for the complete saturation of solution. Then, the specimens were monotonically loaded at different constant load-line displacement rates up to a given final load-line displacement (v_f). After that, the displacement was kept on hold for at least 8 h. Initially, the main objective of maintaining the displacement on hold for a certain time was to analyze the crack behavior under constant displacement. Considering this, in the first tests the hold period was long ($\approx$ 50 h). After some tests it was realized that such long hold times were not necessary anymore. Thus, the hold period was redefined to be between 8 and 12 h based on the laboratory and workers schedule. All the loading sequence, including the hold time, was made with the specimens immersed in the aggressive solution.

Specimens were tested in an Instron 3382 electromechanical testing machine, with a ± 100 kN load cell. In all cases load, actuator displacement, time and DCPD values were digitally recorded. The experimental setup is presented in Fig. 4, which shows the SE(B) specimen already immersed in the aggressive solution, including the plugged DCPD wires.

2.3. Crack growth measurement

As mentioned, the crack length was monitored by DCPD method, which provides continuous crack size measurements during the tests. In this technique, a constant direct current passes through the specimen and the change in the electric resis-

Table 1
Chemical composition of the studied X65 pipeline steel (% weight).

C	Si	Mn	P	S	Cu	Ni	Cr	Mo	Al	Fe
0.059	0.336	1.500	0.019	<0.01	0.042	0.0026	0.106	0.018	0.061	Balance

Table 2
Tensile properties of the studied material.

Direction	σ_{YS} (MPa)	σ_U (MPa)
Longitudinal	477.3	538.6
Transversal	523.9	547.0

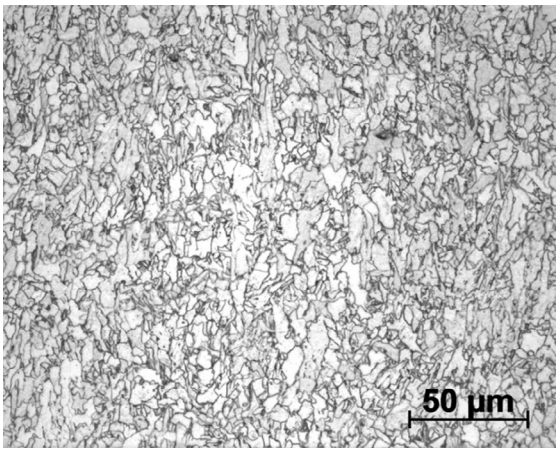

Fig. 2. Microstructure of the tested material showing a fine ferritic microstructure. Etched with 2% Nital solution.

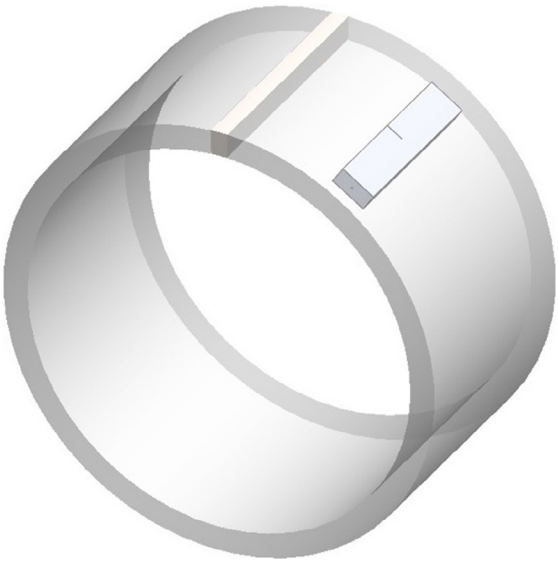

Fig. 3. Schematic representation of SE(B) specimen in L-C orientation.

tance across the remaining ligament is measured. As crack propagates, the remaining ligament diminishes, less area is available for the current flow and the effective resistance increases. As a result, the electric potential drop between the crack faces increases [14,15]. This change in potential drop can be then related to crack length through analytical relationships [14,16]. The Johnson's equation (Eq. (1)) is one of the most known and widely used equation to convert the potential drop measurement into crack size [14,15,17–19].

$$a = \frac{2W}{\pi}\cos^{-1}\frac{\cosh(\pi y/2W)}{\cosh\left\{\left(\frac{U}{U_0}\right)\cosh^{-1}\left[\frac{\cosh(\pi y/2W)}{\cos(\pi a_0/2W)}\right]\right\}} \tag{1}$$

The DCPD method offers several advantages in monitoring crack extension during *J*-R curve tests, which include continuous record of crack size; reduction of time test execution (since it does not require unloading compliance measurements), and the possibility to be used at extreme displacement rates and temperatures [14,15]. However, this method presents some

Fig. 4. Test device showing (a) the specimen positioned in the three-point bending device without test solution, with the plugged DCPD wires, and (b) the specimen immersed in the aggressive environment ready to be tested.

limitations that need to be considered. One limitation refers to the plastic deformation of the ligament that occurs during monotonic loading. This effect, that was also observed during the calibration tests on blunt notch specimens tested in air, amplifies the potential drop signal and could consequently overestimate the crack length [20–22]. This limitation can be solved through corrections by plasticity. On the other hand, when used in electrolytes, care need to be taken to evaluate possible current diverts in the solution which can affect the DCPD values [8,9]. The previous experimental calibration tests in air and in the specific corrosive environment showed that this problem was not present. Finally, some limitations are related to difficulty to distinguish apparent crack growth due to blunting from the stable crack growth in the DCPD records [15,17,19,22].

In this work, the current input and voltage measurement wires were mechanically fastened in the SE(B) specimens through pins. To protect the integrity of electric contact points wires/specimen, an epoxy anticorrosive coating was applied. An Agilent E3633A power supply was used to provide direct current input of 18 A during the tests, and an Agilent 3458A multimeter, with maximum sensitivity of 10 nV, connected to a computer was used to acquire the potential drop data during the tests. The current input was set at 18 A to have a good signal to noise ratio and to avoid thermoelectric effects in the specimen.

2.4. J-R curves evaluation

J-Integral values at each acquisition point corresponding to v and P on the P-v records were calculated as:

$$J_{(i)} = J_{el(i)} + J_{pl(i)} = \frac{K^2_{I(i)}}{E} + \frac{\eta A_{pl(i)}}{B(W - a_{(i)})}, \tag{2}$$

where η = 1.9 for SE(B) specimen, since load-line displacement records were used [11].

The crack length at each load point was obtained by DCPD records, according to Eq. (1). The initial and final crack lengths were optically measured after cryogenic fracture of specimen remaining ligament. In some cases, post-fatigue was used to clearly define the final crack length.

3. Results and discussion

3.1. P-v records

Table 3 summarizes the main test parameters for each specimen. The tests were carried out under different nominal displacement rates, and at the final load-line displacement (v_f) the samples were kept on hold for a given time. The nominal displacement rates refer to the values used during the testing machine set up. However, since nominal displacement values

Table 3
Final displacement and displacement rates for the tested specimens.

Specimen ID	Environment	a_0/W	v_f (mm)	Nominal displacement rate (mm/s)	Actual displacement rate (mm/s)
BM-S-001	Sour*	0.55	2.6	1.0×10^{-5}	0.9×10^{-5}
BM-S-008	Sour*	0.53	2.2	8.0×10^{-5}	5.9×10^{-5}
BM-S-028	Sour*	0.53	7.4	28.0×10^{-5}	25.7×10^{-5}
BM-S-056	Sour*	0.50	7.1	56.0×10^{-5}	49.3×10^{-5}
BM-A-833	Air	0.51	11.9	833.0×10^{-5}	801.0×10^{-5}

* *Sour*: seawater solution saturated with 25% H_2S, balanced CO_2, pH approximately 5, at room temperature and atmospheric pressure.

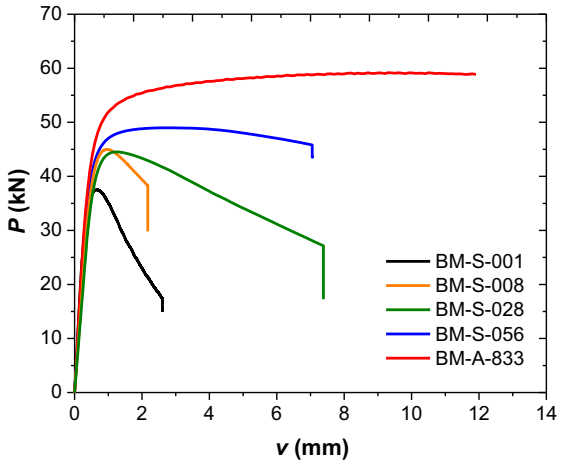

Fig. 5. *P-v* records of all specimens at different displacement rates, including the record of the sample tested in air.

contained spurious components due to the lack of machine stiffness, the actual (average) displacements rates, obtained by the quotient of final load-line displacement (v_f) and the duration of monotonic loading, were consequently lower, as shown in Table 3. Fig. 5 shows load vs. load-line displacement (*P-v*) records of all specimens. For comparison purpose, the *P-v* record of one specimen tested in air (red[1] line) was also included in the Figure. As can be seen there is a tendency of reduction of the maximum load as the displacement rate reduces, even for specimens having similar a_0/W ratios.

As stated in the literature [23], sometimes DCPD method estimates final crack lengths having differences to the physical ones (approximately 5% in this case, as shown in Table 4). Considering this, the final crack lengths estimated through potential drop were linearly corrected with the aim to force those values to match the physical ones [16,23].

3.2. P-t and a-t records

Fig. 6 presents experimental P-*t* and DCPD-*t* records of a SE(B) specimen tested in the specific sour solution. There are three typical regions. In region A, during monotonic loading, there is an increase in the DCPD values, which corresponds to crack growth, as usual in monotonic loading tests. The region C corresponds to the unloading condition (zero load), where DCPD values remain constant and no crack growth is expected, because no crack driving force is applied. Finally, the region B corresponds, in this case, to a constant displacement condition. There are three possible behaviors of load and DCPD signals in the region B:

(1) applied load and DCPD values remain constant;
(2) applied load decreases and DCPD values increase immediately after hold; or
(3) applied load and DCPD values remain constant for a certain time (defined as incubation time), followed by decreasing in applied load and increasing in DCPD values.

By definition, constant DCPD values indicate no crack growth. For this geometry under constant displacement condition increasing DCPD values and decreasing loads are associated to subcritical crack growth by stress corrosion cracking [24]. From the point of view of crack growth mechanisms, the combined behavior of applied load and DCPD values in region B is very important. As already mentioned, the incubation period was associated to constant DCPD values in region B.

[1] For interpretation of color in Fig. 5, the reader is referred to the web version of this article.

Table 4
Original and physical crack sizes, and final crack sizes estimated by DCPD.

Specimen ID	a_0 (mm)	a_p (mm)	a_{PD} (mm)	a_p–a_{PD} (%)
BM-S-001	26.48	38.23	36.49	4.55
BM-S-008	25.42	31.98	30.18	5.63
BM-S-028	25.23	36.64	34.80	5.02
BM-S-056	23.95	27.03	26.91	0.44

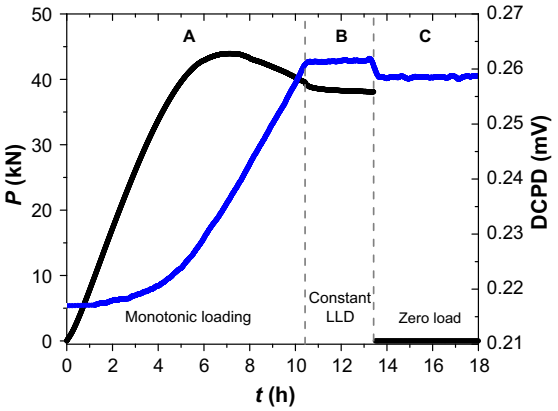

Fig. 6. Typical DCPD vs. time t records of specimen tested in the specific solution.

Figs. 7–10 show the *P*-*t* and *a*-*t* records of all specimens. Focusing on *a*-*t* records, from Fig. 7 it is possible to see that for specimen BM-S-001, when v_f was kept on hold at the end of monotonic test, crack continued to growth without increasing in driving force, which is a clear evidence of subcritical crack growth without incubation time (situation 2 in region B of Fig. 6). The curves in Figs. 8 and 9 correspond to specimens BM-S-008 and BM-S-028, respectively. In these two tests, it is also possible to see crack growth at constant displacement, but in these cases incubation time was present prior the beginning of subcritical crack growth (situation 3 in region B of Fig. 6). Finally, for sample BM-S-056, tested with nominal displacement rate of 56.0×10^{-5} mm/s and kept on hold at $v_f = 7.1$ mm (see Fig. 10), no evidence of subcritical crack growth was observed (situation 1 in region B of Fig. 6).

Focusing on the *P*-*t* records shown in Figs. 7–10, it is possible to see that load behavior during hold period for all specimens is coherent with discussion above. Immediately after hold there was a load relaxation and then its stabilization. After that, load fell continuously due to subcritical crack growth. That load drop after relaxation occurred only in the cases where subcritical crack growth was present (with or without incubation time). This *P*-*t* curve behavior is well known and it is typical of subcritical growth existence when specimens are loaded under constant displacement. In the ASTM F1624 standard [25], that load drop is used as a criterion for the definition of the load at which crack growth initiates. Hydrogen embrittle-

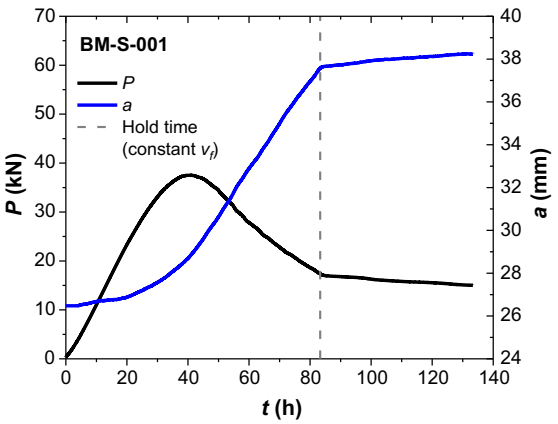

Fig. 7. *P*-*t* and *a*-*t* records of specimen BM-S-001.

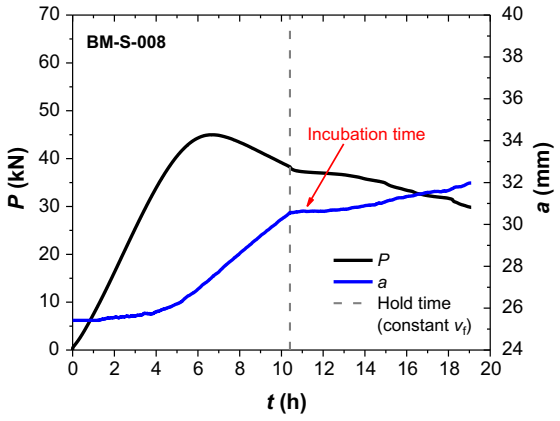

Fig. 8. *P-t* and *a-t* records of specimen BM-S-008.

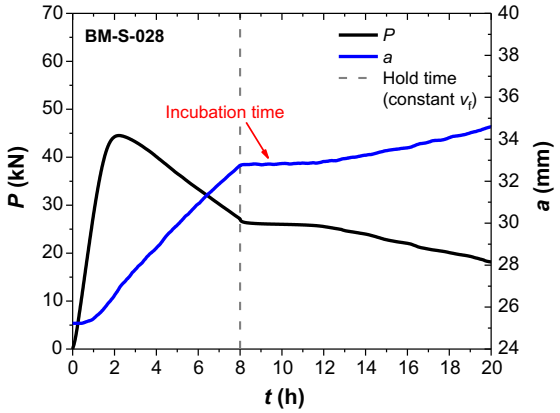

Fig. 9. *P-t* and *a-t* records of specimen BM-S-028.

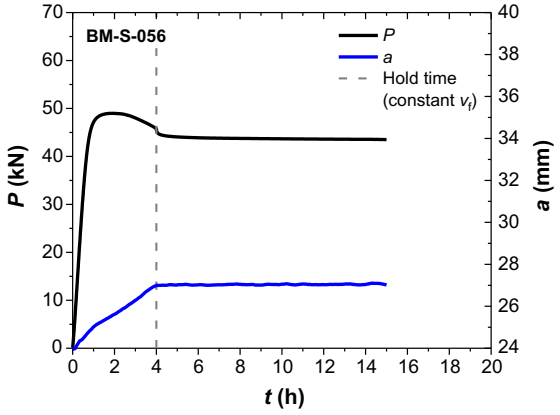

Fig. 10. *P-t* and *a-t* records of specimen BM-S-056.

ment threshold of steels is measured by incremental step loading through this method (type A and C records shown in Fig. 11).

Table 5 presents total test duration, monotonic test duration, crack extension during monotonic loading, incubation time, and physical crack extension measured after cryogenic fracture and/or post-fatigue. As said, specimen BM-S-001 did not

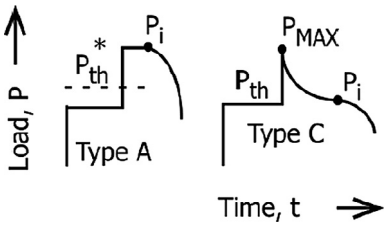

Fig. 11. Profiles of load drop for definition of crack initiation load (P_i) and threshold load (P_{th}), in the Incremental Step Loading Technique [25]. Profiles of type A and C are indicative of subcritical crack growth. Adapted from [25].

Table 5
Testing times and crack extensions for all specimens.

Specimen ID	Total test duration (h)	Monotonic test duration (h)	Monotonic Δa_{PD} (mm)	Incubation time (h)	Total Δa_p (mm)
BM-S-001	133.33	83.33	11.04	0.00	11.75
BM-S-008	19.09	10.41	5.14	1.67	6.56
BM-S-028	20.71	8.00	8.95	4.48	11.41
BM-S-056	15.00	4.00	3.01	>11.00	3.08

show incubation time. On the other hand, the large crack growth on this specimen that can be seen in Fig. 12a corroborates the evidence of subcritical crack growth during monotonic loading. For specimen BM-S-056, the time on hold cannot be considered as incubation time, since subcritical crack growth was not observed, as seen from crack extension values at the end of monotonic loading and at the end of test (Table 5). For the other nominal displacement rates tested (8.0×10^{-5} mm/s and 28.0×10^{-5} mm/s), which presented incubation time before beginning of subcritical crack growth, the results suggested that these mechanisms can be separated. At these nominal displacement rates the crack extension seemed to be stable during the

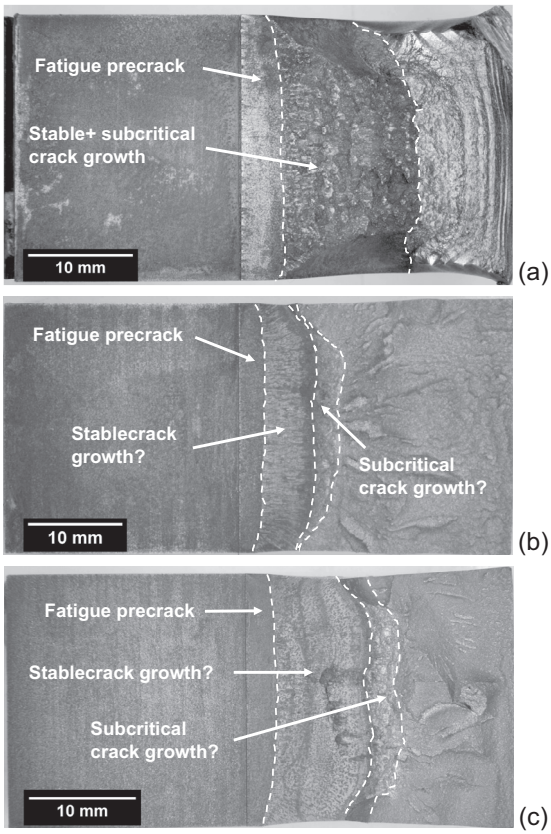

Fig. 12. Fracture surfaces: (a) specimen BM-S-001 (no incubation time); (b) specimen BM-S-008 (8.68 h on hold and approximately 1.7 h of incubation time); (c) specimen BM-S-028 (12.71 h on hold and approximately 4.5 h of incubation time).

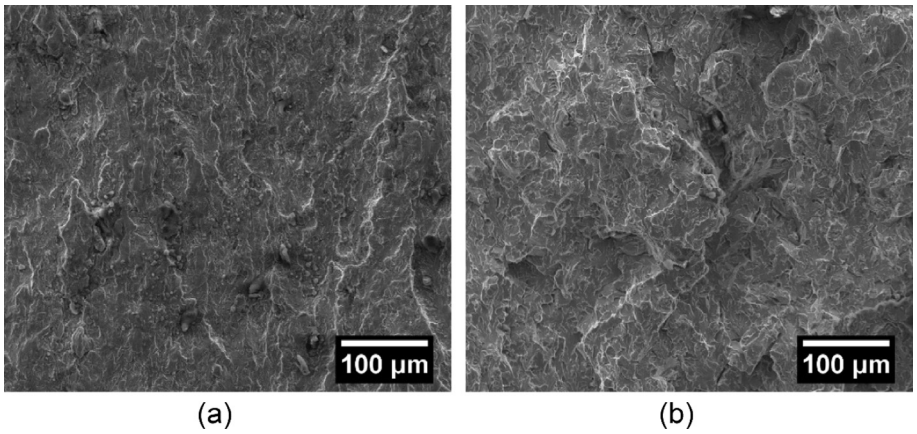

Fig. 13. SEM analysis of fracture surface of specimen BM-S-008, indicating supposed regions of stable crack growth (a) and subcritical crack growth (b).

monotonic part of the test, and after the incubation period, the crack growth was only by a subcritical mechanism (without increasing in driving force).

3.3. Fractures surfaces and crack path

Stereographic microscope observations of fracture surface of specimens BM-S-008 and BM-S-028 (Fig. 12b and c, respectively) revealed different regions, that could be associated to stable and/or subcritical crack growth regimes. SEM observations of these regions, as can be seen in Fig. 13, did not show any conclusive difference. To elucidate the crack propagation mechanism (intergranular or transgranular) in these regions, SEM analysis was performed in the perpendicular plane to the fracture surface in the center of the specimen (Fig. 14). As can be seen, the grain size is very small, which makes it more difficult to analyze, but in region of supposed stable crack growth the crack propagation is transgranular, whereas in the supposed subcritical crack growth region the mechanism seems to be intergranular. More analysis need to be done for elucidating this point.

3.4. J-R curves

Experimental J-R curves were evaluated according to ASTM E1820 standard [11]. Fig. 15 presents all the experimental J-Δa pairs, the qualified pairs for J-R curve fitting, and the fitted curves of tested specimens. In air this steel behaves as very tough material, with J-Δa pairs following the blunting line. In the specific sour environment the material resistance to crack growth was highly reduced. The results also showed an expected behavior in this environment where lower load-line displacement rates led to lower J-R curves. As mentioned previously, and according to literature [5–7], when the material is

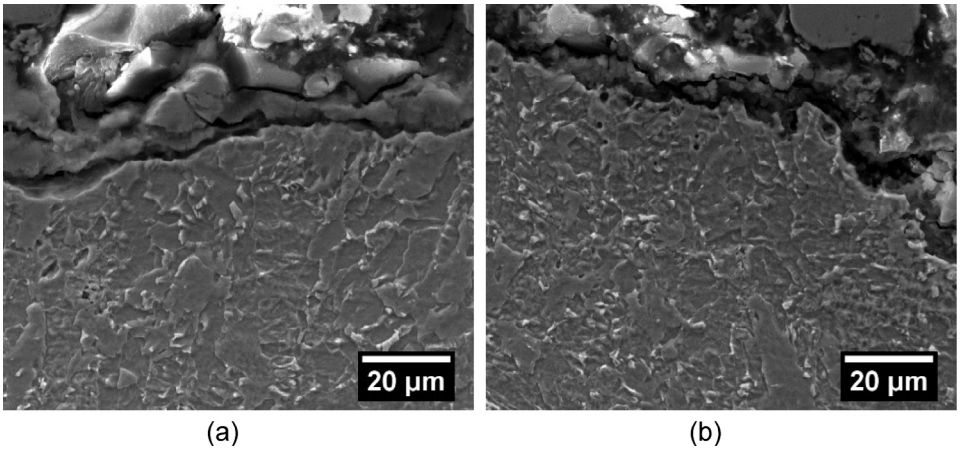

Fig. 14. SEM analysis at transversal section of crack surface of specimen BM-S-028, showing crack propagation mechanisms at supposed regions of stable crack growth (a), and subcritical crack growth (b).

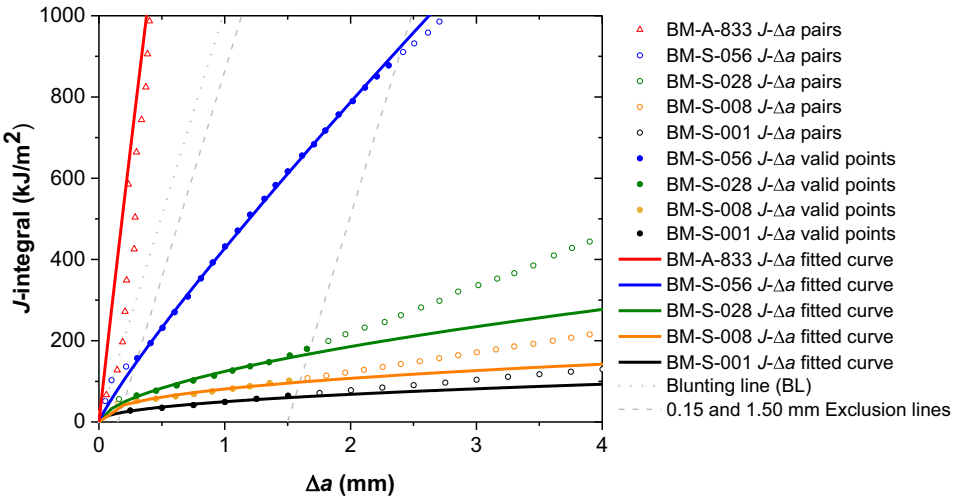

Fig. 15. *J*-Δ*a* pairs and fitted *J*-R curves of tested specimens.

tested under low displacement rates, the exposure time to aggressive environment is longer, and this affects the material resistance to crack growth. The results corroborated the expected *J*-R curve dependency on the displacement rate.

According to *P*-*t* and *a*-*t* records, the occurrence of subcritical crack growth without incubation time for test carried out at a very low nominal displacement rate (1.0×10^{-5} mm/s) indicates that the mechanisms of stable and subcritical crack growth coexist and may interact during the test. Otherwise, for the other nominal displacement rates tested in this work, the subcritical crack growth was only detectable after an incubation period, which may indicate the possibility to dissociate both mechanisms. Thus, it is possible that under certain displacement rates the material will feature a "true" *J*-R curve, which is not affected by subcritical crack growth mechanism. According to the results of this work, the nominal displacement rate that should be used to characterize this material in that environment seems to be near 8.0×10^{-5} mm/s, since it presented the smaller incubation time, indicating that there was only stable crack extension along the region A of the test.

As a proposal, for *J*-R curves experimental assessment and fracture toughness values of a given steel in a specific aggressive environment the experimental procedure shall consider performing the monotonic test under displacement control, and at the end of monotonic loading (region A of Fig. 6) keep displacement on hold for some time while crack length is continuously monitored (region B of Fig. 6). If crack continues to growth at that constant displacement without incubation time, the evaluated *J*-R curve is influenced by subcritical crack growth. On the other hand, if an incubation time is present, the evaluated *J*-R curve seems to have only the contribution of stable crack growth. Repeating this loading profile for different displacement rates, an appropriate one to evaluate *J*-R curves without contribution of subcritical crack growth could be defined.

4. Conclusions

Results showed that this sour environment reduced the material resistance to crack growth. This behavior was strongly affected by displacement rate. As it decreased, *J*-R curves were lower, and material fracture toughness dropped.

When tested at the lowest nominal displacement rate (1.0×10^{-5} mm/s) the experimental *J*-R curve had contribution of subcritical crack growth. For nominal displacements rates of 8.0×10^{-5} mm/s and above, there was no evidence of subcritical crack growth during the tests. Although more research need to be done, the mechanism of stable and/or subcritical crack growth seems to be separable. As can be inferred, certain experimental displacement rate would separate the occurrence of both or just one mechanism.

To evaluate the contribution or not of subcritical crack growth on *J*-R curves of carbon steels when immersed in a specific aggressive environment, it is proposed that, at the end of the monotonic part of the test, the final displacement v_f be kept on hold for a certain time, and the crack length being continuously monitored. In the absence of crack growth at constant displacement and/or in the presence of an incubation time before this crack growth, the evaluated *J*-R curve can be considered free of subcritical crack growth contribution.

Acknowledgements

To Tenaris Confab and the Brazilian Agency for Industrial Research and Innovation (Embrapii) for the financial support. To CNPq for the scholarship of C. Finamore. To João T.O. de Menezes, Leandro M. Morani, and Rafael F. Barrozo for the technical support.

References

[1] Iannuzzi M. Environmentally assisted cracking (EAC) in oil and gas production. In: Raja VS, Shoji T, editors. Stress corrosion cracking: theory and practice. Woodhead Publishing; 2011. p. 570–607.
[2] Bell JM, Chin YD, Hanrahan S. State-of-the-art of ultra deepwater production technologies. In: Offshore technology conference, OTC 17615, Houston, TX; 2005.
[3] Zhao MC, Yang K, Shan Y-Y. The effects of thermo-mechanical control process on microstructures and mechanical properties of a commercial pipeline steel. Mater Sci Eng A 2002;335:14–20.
[4] Chong TS, Kumar SB, Lai MO, et al. Effects of wet H_2S containing environment on mechanical properties of NACE grade C-Mn steel pipeline girth welds. Eng Fract Mech 2014;131. 485-03.
[5] Dietzel W, Schwalbe K-H. A study of the hydrogen induced stress corrosion cracking of a low alloy steel using fracture mechanics techniques. In: Moody NR, Thompson AW, editors. Hydrogen effects on material behavior. The Minerals, Metals & Materials Society; 1990. p. 975–83.
[6] Dietzel W. Rising displacement stress corrosion cracking testing. Metall Mater Trans A 2011;42A:365–72.
[7] Dietzel W, Schwalbe K-H. Application of the rising displacement test to SSC investigations. In: Kane RD, editor. ASTM STP 1210 – slow strain rate testing for the evaluation of environmentally induced cracking: research and engineering applications. West Conshohocken, USA: American Society for Testing and Materials; 1993. p. 134–48.
[8] Dietzel W, Bala Srinivasan P, Atrens A. Testing and evaluation methods for stress corrosion cracking (SCC) in metals. In: Raja VS, Shoji T, editors. Stress corrosion cracking: theory and practice. Woodhead Publishing; 2011. p. 133–66.
[9] Dietzel W, Atrens A, Barnoush A. Mechanics of modern test methods and quantitative-accelerated testing for hydrogen embrittlement. In: Gangloff RP, Somerday B, editors. Gaseous hydrogen embrittlement of materials in energy technologies, vol. 1. Woodhead Publishing; 2012. p. 237–73.
[10] ASTM E8/E8M. Standard test methods for tension testing of metallic materials. West Conshohocken, USA: American Society for Testing of Materials; 2016.
[11] ASTM E1820. Standard Test Method for Measurement of Fracture Toughness. West Conshohocken, USA: American Society for Testing of Materials; 2016.
[12] BS 7448: Part 1. Fracture mechanics toughness tests – method for determination of KIC, critical CTOD and critical J values of metallic materials. London, UK: British Standards Institution; 1991.
[13] ASTM D1141. Standard practice for the preparation of substitute ocean water. West Conshohocken, USA: American Society for Testing of Materials; 2013.
[14] Chen X, Nanstad RK, Sokolov MA. Application of direct current potential drop for the J-integral vs. Crack growth resistance curve characterization. In: ASTM STP 1584 – evaluation of existing and new sensor technologies for fatigue, fracture and mechanical testing. West Conshohocken: American Society for Testing of Materials; 2015. p. 97–112.
[15] Marschall CW, Held PR, Landow MP, Mincer PN. Use of the direct-current electric potential method to monitor large amounts of crack growth in highly ductile metals. In: Gudas JP, Joyce JA, Hackett EM, editors. ASTM STP 1074 – fracture mechanics; twenty-first symposium. West Conshohocken: American Society for Testing of Materials; 1990. p. 581–593.
[16] ASTM E647. Standard test method for measurement of fatigue crack growth rates. West Conshohocken, USA: American Society for Testing of Materials; 2015
[17] Landow MP, Marschall CW. Experience in using direct current electric potential to monitor crack growth in ductile metals. In: Joyce JA, editor. ASTM STP 1114 – elastic-plastic fracture test methods: the user's experience (second volume). West Conshohocken: American Society for Testing of Materials; 1991. p. 163–77.
[18] Schwalbe K-H, Hellmann D, Heerens J, et al. Measurement of stable crack growth including detection of initiation of growth using the DC potential drop and the partial unloading methods. In: Wessel ET, Loss FJ, editors. ASTM STP 856 – elastic-plastic fracture test methods: the user's experience. West Conshohocken: American Society for Testing of Materials; 1985. p. 338–62.
[19] ISO 12135: metallic materials – unified method of test for the determination of quasi-static fracture toughness. Switzerland: International Standards Organization (ISO); 2016.
[20] Wilkowski GM, Maxey WA. Review and applications of the electric potential method for measuring crack growth in specimens, flawed pipes, and pressure vessels. In: Lewis JC, Sines G, editors. ASTM STP 791 – fracture mechanics: fourteenth symposium – vol II: testing and applications. West Conshohocken: American Society for Testing of Materials; 1983. p. II-266–II-294.
[21] Okumura N, Venkatasubramanian TV, Unvala BA, Baker TJ. Application of the AC potential drop technique to the determination of *R* curves of tough ferritic steels. Eng Fract Mech 1981;14:617–25.
[22] Konosu S, Shimazu H, Fukuda R. Tearing resistance properties of Cr-Mo steels with internal hydrogen determined by the potential drop method. Metall Mater Trans A 2015;46A:5626–37.
[23] Nibur KA, Somerday BP, Marchi CS, et al. The relationship between crack tip strain and subcritical cracking thresholds for steels in high-pressure hydrogen gas. Metall Mater Trans A 2013;44A:248–69.
[24] Wei RP. Fracture mechanics - integration of mechanics, materials science, and chemistry. USA: Cambridge University Press; 2010.
[25] ASTM F1624. Standard test method for measurement of hydrogen embrittlement threshold in steel by the incremental step loading technique. West Conshohocken, USA: American Society for Testing of Materials; 2012.